Super-resolution Imaging of the Protoplanetary Disk HD 142527 Using Sparse Modeling

Masayuki Yamaguchi,[1,2] Kazunori Akiyama,[2,3,4,5], Akimasa Kataoka[2,7], Misato Fukagawa[2,7], Takashi Tsukagoshi[2], Takayuki Muto[9], Shiro Ikeda[6], Mareki Honma[2,7], Ryohei Kawabe[1,2,7]

[1]*Department of Astronomy, Graduate School of Science, The University of Tokyo, 7-3-1 Hongo, Bunkyo-ku, Tokyo 113-0033, Japan;*
masayuki.yamaguchi@nao.ac.jp

[2]*National Astronomical Observatory of Japan, 2-21-1 Osawa, Mitaka, Tokyo 181-8588, Japan*

[3]*National Radio Astronomy Observatory, 520 Edgemont Rd, Charlottesville, VA 22903, USA*

[4]*Massachusetts Institute of Technology, Haystack Observatory, 99 Millstone Rd, Westfod, MA 01886, USA*

[5]*Black Hole Initiative, Harvard University, 20 Garden Street, Cambridge, MA 02138, USA*

[6]
The Institute of Statistical Mathematics, 10-3 Midori-cho, Tachikawa, Tokyo 190-8562, Japan

[7]*Department of Statistical Science, School of Multidisciplinary Sciences, Graduate University for Advanced Studies, 10-3 Midori-cho, Tachikawa, Tokyo 190-8562, Japan*

[8]*Department of Astronomical Science, School of Physical Sciences, Graduate University for Advanced Studies, 2-21-1 Osawa, Mitaka, Tokyo 181-8588, Japan*

[9]*Division of Liberal Arts, Kogakuin University, 1-24-2 Nishi-Shinjuku, Shinjuku-ku, Tokyo 163-8677, Japan*

Abstract. High-resolution observations of protoplanetary disks with radio interferometers are crucial for understanding the planet formation process. Recent observations using Atacama Large Millimeter/submillimeter Array (ALMA) have revealed various small-scale structures in disks. In interferometric observations, the observed data are an incomplete set of Fourier components of the radio source image. The image reconstruction is therefore essential in obtaining the images in real space. The CLEAN technique has been widely used, but recently, a new technique using the sparse modeling approach is suggested. This technique directly solves a set of undetermined equations and has been shown to behave better than the CLEAN technique based on mock observations with VLBI (Very Long Baseline Interferometry). However, it has never been applied to ALMA-like connected interferometers nor real observational data. In this work, for the first time, the sparse modeling technique is applied to observational

data sets taken by ALMA. We evaluate the performance of the technique by comparing the resulting images with those derived by the CLEAN technique. We use two sets of ALMA archival data at Band 7 (∼ 350 GHz) for the protoplanetary disk around HD 142527. One is taken in the intermediate-baseline array configuration, and the other is in the longer-baseline array configuration. The image resolutions reconstructed from these data sets are different by a factor of ∼ 3. We compare images reconstructed using sparse modeling and CLEAN. We find that the sparse modeling technique can successfully reconstruct the overall disk emission. The previously known disk structures appear on both images made by the sparse modeling and CLEAN at its nominal resolutions. Remarkably, the image reconstructed from intermediate-baseline data using the sparse modeling technique matches very well with that obtained from longer-baseline data using the CLEAN technique.

1. Introduction

Finer resolution with radio interferometers providing a more detailed picture of disk structure can constrain their evolution and establish the framework of this type. Recent observations using Atacama Large Millimeter/submillimeter Array (ALMA) have revealed various small-scale structures in disks. In interferometric observations, images of astronomical source $I(l, m)$ can be obtained by two-dimensional Fourier transform of observed data $V(u, v)$. However, in practical observation, there must be space between antennas, which causes unsampled holes in the (u, v) plane. Such an incomplete (u, v) coverage always causes “underdetermined problem” in the radio interferometer equation. Usually, this problem is solved by filling unsampled visibilities with zero. However, this process causes the resultant image to be “dirty image”.

2. Imaging Techniques for Radio Interferometer

2.1. Imaging with CLEAN

CLEAN (Högbom 1974) is a most common algorithm in radio astronomy and uses nonlinear techniques effectively interpolate sample of $V(u, v)$ into unsampled regions of the (u, v) plane. The algorithm assumes that the image consists of many point sources and is, therefore, to break down the intensity distribution in the dirty image into point source responses, and then replaces each one with the Gaussian with a half-amplitude width equal to that of the original synthesized beam. This procedure finally provides a CLEAN image, but there is a limitation of the nominal resolution (diffraction limit) defined by the maximum length of the baseline between two telescopes. In this works, multi-scale Cotton-Schwab CLEAN (henceforth MS-CLEAN; Wakker & Schwarz (1988)) is adopted as the image reconstruction.

2.2. Imaging with Sparse Modeling

For the imaging with sparse modeling, ℓ_1+TSV regularization (Kuramochi et al. 2018) is adopted as the regularization function of the image reconstruction. The equation becomes a convex optimization, guaranteeing the global convergence to a unique solution regardless of initial conditions by choosing the meaningful sparse image from the infinite number of possible solutions by introducing two regularization terms: the ℓ_1 norm

and Total Squared Variation (TSV) of the brightness distribution (see Akiyama et al. 2017b; Kuramochi et al. 2018, for details), and can achieve an optimal resolution of $\sim$ 30% of the diffraction limit ($\sim$ 3 time better angular resolution) by adjusting two positive variables Λ_ℓ and Λ_t in these two regularization terms. Λ_ℓ and Λ_t can effectively be determined by evaluating goodness-fitting with 10- fold cross validation (e.g., Honma et al. 2014; Akiyama et al. 2017a,b; Kuramochi et al. 2018)

2.3. Analysis

We adopted two data sets of ALMA observations toward the protoplanetary disk HD 142527 at close frequencies in Band 7 using different array configurations. The maximum baseline lengths of these data sets differ by a factor of $\sim$3. Throughout this paper, we name the data set obtained with the more compact (i.e., intermediate-baseline) array configuration as *Data 1*, while that from the more extended (i.e., longer-baseline) one as *Data 2*. In below, we summarize observations for each data set. Data 1 was obtained as part of the project 2015.100425.S, which are already reported in Kataoka et al. (2016). The corresponding observations were carried out on March 11, 2015, at 343 GHz (0.87 mm) and at full polarizations. The observing array consisted of thirty-eight 12 m antennas, providing the longest projected baseline length of 460 m. Data 2 were obtained as part of project 2012.1.00631.S on 2015 July 17 at 322 GHz (0.93 mm) and at dual polarizations. Observations made use of forty 12 m antennas with the longest projected baseline length of 1570 m. For the data sets, We compare images reconstructed by sparse modeling and CLEAN.

3. Results

3.1. Image Appearance at Different Angular Resolution

As shown in Figure 1, we find that the sparse modeling technique can successfully reconstruct the overall disk emission. The previously known disk structures appear on both images made by the sparse modeling and CLEAN at its nominal resolutions. Remarkably, the image reconstructed from Data 1 using the sparse modeling technique matches very well with that obtained from Data 2 using the CLEAN technique with the accuracy of $\sim$ 90% on the image domain (see, the third panel of Figure 1).

4. Conclusion

We have shown that the sparse modeling technique is potentially useful in actual data analyses and may improve the spatial resolution by a factor of 3.

References

Akiyama, K., Ikeda, S., Pleau, M., Fish, V. L., Tazaki, F., Kuramochi, K., Broderick, A. E., Dexter, J., Mościbrodzka, M., Gowanlock, M., Honma, M., & Doeleman, S. S. 2017a, AJ, 153, 159. 1702.00424

Akiyama, K., Kuramochi, K., Ikeda, S., Fish, V. L., Tazaki, F., Honma, M., Doeleman, S. S., Broderick, A. E., Dexter, J., Mościbrodzka, M., Bouman, K. L., Chael, A. A., & Zaizen, M. 2017b, ApJ, 838, 1. 1702.07361

Beck, A., & Teboulle, M. 2009a, Image Processing, IEEE Transactions on, 18, 2419

— 2009b, SIAM journal on imaging sciences, 2, 183
Birdi, J., Repetti, A., & Wiaux, Y. 2018, ArXiv e-prints. 1801.02417
Boehler, Y., Weaver, E., Isella, A., Ricci, L., Grady, C., Carpenter, J., & Perez, L. 2017, ApJ, 840, 60. 1704.00787
Chael, A. A., Johnson, M. D., Narayan, R., Doeleman, S. S., Wardle, J. F. C., & Bouman, K. L. 2016, ApJ, 829, 11. 1605.06156
Högbom, J. A. 1974, A&AS, 15, 417
Honma, M., Akiyama, K., Uemura, M., & Ikeda, S. 2014, PASJ, 66, 95
Kataoka, A., Tsukagoshi, T., Momose, M., Nagai, H., Muto, T., Dullemond, C. P., Pohl, A., Fukagawa, M., Shibai, H., Hanawa, T., & Murakawa, K. 2016, ApJ, 831, L12. 1610.06318
Kuramochi, K., Akiyama, K., Ikeda, S., Tazaki, F., Fish, V. L., Pu, H.-Y., Asada, K., & Honma, M. 2018, ApJ, 858, 56
Thompson, A. R., Moran, J. M., & Swenson, G. W., Jr. 2017, Interferometry and Synthesis in Radio Astronomy, 3rd Edition
Wakker, B. P., & Schwarz, U. J. 1988, A&A, 200, 312

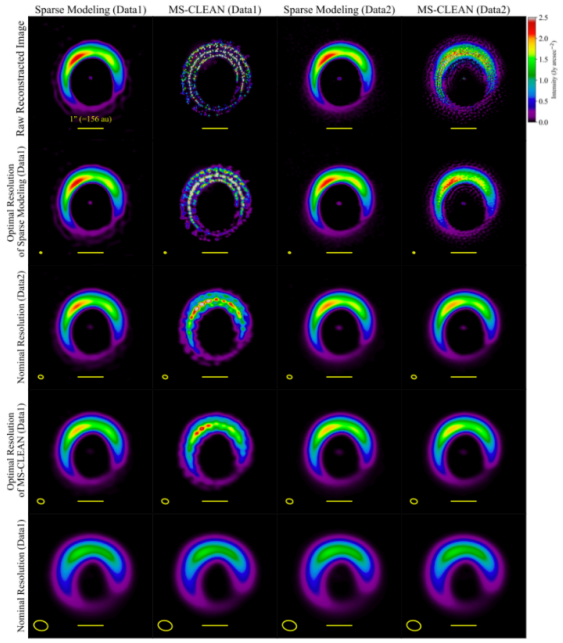

Figure 1. Images of HD 142527 from two datasets of ALMA observations at Data 1 and Data 2 reconstructed with sparse modeling and MS-CLEAN. The left two columns show images from Data 1 reconstructed with sparse modeling and MS-CLEAN, respectively, while the right two columns show images from Data 2 as well. Each row shows raw reconstructed images or those restored with an elliptical Gaussian beam, whose FWHM shape is shown in a yellow ellipse in each panel. (2nd/4th panels): Reconstructed images convolved with the optimal beam of Data 1 for sparse modeling and MS-CLEAN, respectively, determined by NRMSE analysis (Chael et al. 2016; Akiyama et al. 2017b; Kuramochi et al. 2018). (3rd/5th panels): Reconstructed images convolved with the nominal beams, which have the same solid angles same to the synthesized beam of Data 1 and 2, respectively, for the above Briggs weighting.